

# Minimal Single-Particle Hamiltonian for Charge Carriers in Epitaxial Graphene on 4H-SiC (0001)

Seungchul Kim,<sup>1</sup> Jisoon Ihm,<sup>1</sup> Hyoung Joon Choi,<sup>2</sup> and Young-Woo Son<sup>3,y</sup>

<sup>1</sup>Department of Physics and Astronomy, Seoul National University, Seoul 151-747, Korea

<sup>2</sup>Department of Physics and IPAP, Yonsei University, Seoul 120-749, Korea

<sup>3</sup>Korea Institute for Advanced Study, Seoul 130-722, Korea

(Dated: February 22, 2024)

We present a minimal but crucial microscopic theory for epitaxial graphene and graphene nanoribbons on the 4H-SiC (0001) surface (prototypical materials to explore physical properties of graphene in large scale). Coarse-grained model Hamiltonians are constructed based on the atomic and electronic structures of the systems from first-principles calculations. From the theory, we unambiguously uncover origins of several intriguing experimental observations such as broken-symmetry states around the Dirac points and new energy bands arising throughout the Brillouin zone, thereby establishing the role of substates in modifying electronic properties of graphene. We also predict that armchair graphene nanoribbons on the surface have a single energy gap of 0.2 eV when their widths are over 15 nm, in sharp contrast to their usual family behavior.

PACS numbers: 73.20.-r, 81.05.Uw, 68.35.-p, 71.20.-b

Graphene has attracted immense interests because of the unusual relativistic energy dispersions with the chiral massless Dirac fermions near the Fermi level ( $E_F$ ) [1, 2, 3]. The direct observation of such peculiar quasiparticle spectra in graphene is particularly important not only for understanding its novel physical properties [2, 3, 4, 5] but also for practical applications [4, 5]. So, several measurements through the high resolution angle resolved photoemission spectroscopy (ARPES) are performed on a single layered epitaxial graphene lying on the silicon carbide (0001) surfaces [6, 7, 8, 9, 10]. Surprisingly, the reported quasiparticle spectra reveal anomalous energy dispersions around the Dirac energy point ( $E_D$ ) indicating highly renormalized bands [6] or energy gap [7] there. Many experimental [8, 9, 10, 11, 12, 13, 14, 15, 16, 17, 18] and theoretical studies [19, 20, 21, 22, 23, 24, 25, 26] address these important problems but there is still no consensus on origins of the anomalous spectrum. Moreover, there is no clear understanding on other anomalous ARPES observations such as the broken six-fold symmetry near the  $E_D$  and new distorted hexagonal energy bands around Brillouin zone (BZ) center [6, 7, 8, 9].

The complex interfacial structures arise when epitaxial graphene is grown by annealing SiC surfaces [27]. During the thermal decomposition of the surfaces, a layer of carbon atoms, called the buffer layer, forms first without exhibiting the typical linear energy dispersion of  $\pi$ -states near the  $E_F$  [27, 28, 29, 30]. Then, on top of the buffer layer, the clean honeycomb lattice of carbon atoms grows [27, 28, 29, 30, 31]. The lattice mismatch between the SiC (0001) surface, buffer layer and graphene gives rise to the large scale surface reconstruction with a periodicity of  $6\sqrt{3} \times 6\sqrt{3}$  R30 (in short, 6R3) with respect to the SiC (0001) surface unit cell, which is observed in the low energy electron diffraction (LEED) measurements [27, 28, 29, 30, 31]. The scanning tunnelling mi-

croscopy (STM) image, however, indicates an approximate  $6 \times 6$  periodicity [11, 14, 15, 16] of the reconstruction. We note that such superperiodic rearrangements shall impose constraints on possible theoretical models to explain the anomalous electronic structures mentioned above.

In this paper, we show that the interactions between epitaxial graphene and the reconstructed layer underneath it are the main driving forces to several anomalous features observed in recent experiments [6, 7, 8, 9, 10, 11, 12, 13, 14, 15, 16, 17, 18] on electronic properties of epitaxial graphene. From the simulated ARPES spectra on the systems, it is shown that the symmetry breaking at the  $E_D$  and the new hexagonal bands throughout the two-dimensional BZ have the same origins. Based on the model, we predict that graphene nanoribbons or finite size fragments of graphene [4, 9, 12, 28] show an homogeneous energy gap contrary to their family behavior [32]. Moreover, by extending our microscopic model from monolayer epitaxial graphene to bilayer one, we identify the effects of the buffer layer to its energy spectrum and characteristic energy gap [7, 8, 9, 10, 17]. Our computational results indicate that the interplays between geometries and electronic structures are pivotal in altering global energy bands of graphene, notwithstanding that the many-body interactions [24, 25, 26] are expected to play some roles in modifying the quasiparticle spectrum near the  $E_D$  locally.

From the ab-initio pseudopotential density functional method [22, 33, 34], we find that the carbon atoms in the buffer layer with superperiodic  $6R3$  unit cell are split into lattice matched regions, where carbon atoms have  $\pi$ -bonds to silicon atoms of the 4H-SiC (0001) surface, and their boundaries without the  $\pi$ -bonds [22] (Fig. 1(a)). The carbon atoms at the boundaries of the lattice matched regions exhibit an approximate  $6 \times 6$  domain

satisfying the geometric constraint imposed simultaneously by both LEED and STM measurements. To explore various initial conditions for buffer layer formation, we shift the initial atomic coordinates of the buffer layer (shown in Fig. 1(b)) on top of the 4H-SiC (0001) surface by either  $\frac{1}{2}\mathbf{a}_1$  (Fig. 1(c)) or  $\frac{1}{2}\mathbf{a}_2$  (Fig. 1(d)) where  $\mathbf{a}_{1(2)}$  is a unit vector of graphene. We find that the final relaxed atomic geometries for all initial coordinates are essentially same to each other except for minor differences in the connectivity of  $\pi$ -electrons along quasi-6  $\times$  6 domain boundaries (Figs. 1(b)-(d)).

We build up a minimal (coarse-grained) microscopic model for interactions between epitaxial graphene and the buffer layer based on atomic and electronic structures obtained from our first-principles calculation (See detailed method in [34]). From the first-principles calculations, it is found that the interactions between  $\pi$ -orbital states at the domain boundary of the buffer and ones in graphene play the most significant role to determine the electronic structures of the system while the states of atoms inside the domain and those under the buffer layer have negligible contributions to the electronic structures near the  $E_F$  and  $E_D$ . Hence, it is sufficient to approximate the buffer layer to the coarse-grained atomic configuration of the quasi-6  $\times$  6 periodic connections of  $\pi$ -electrons only (thick black lines in Figs. 1(b)-(d)). Our tight-binding Hamiltonian for monolayer epitaxial graphene on coarse-grained buffer layer model (Fig. 1b) can be written as

$$H = \sum_{\mathbf{r}, \mathbf{r}'} t_G c_{\mathbf{r}}^\dagger c_{\mathbf{r}'} + \sum_{\mathbf{r}, \mathbf{r}'} V_G c_{\mathbf{r}}^\dagger c_{\mathbf{r}'} + \sum_{\mathbf{r}, \mathbf{r}'} t_B b_{\mathbf{r}}^\dagger b_{\mathbf{r}'} + \sum_{\mathbf{r}, \mathbf{r}'} V_B b_{\mathbf{r}}^\dagger b_{\mathbf{r}'} + \sum_{\mathbf{r}, \mathbf{r}'} c_{\mathbf{r}}^\dagger b_{\mathbf{r}'} + \text{c.c.}; \quad (1)$$

where  $t_G$  (2.70 eV) and  $t_B$  (1.50 eV) are the nearest neighbour hopping amplitude between carbon atoms in graphene and those in the buffer layer respectively. The  $c_i$  and  $b_i$  are annihilation operators for electron in graphene and buffer layer respectively. (0.30 eV) denotes the interlayer hopping amplitude between the nearest neighbour carbon atoms belong to graphene and the buffer layer with the Bernal type stacking respectively.  $V_G$  (0.35 eV) and  $V_B$  (0.34 eV) describe the potential for graphene and the buffer layer considering charge redistributions due to the polar SiC surface. Since our model Hamiltonians are described within the single-orbital tight-binding approximation, we can readily extend our model to explore the electronic structures of finite-sized monolayer and multilayer epitaxial graphene respectively which are beyond the reach of the first-principles calculations.

We have found that the nearest neighbour inter- and intra-layer interactions between  $\pi$ -electrons in the coarse-grained atomic model (Eq. (1)) are sufficient to reproduce the electronic energy bands obtained from the first-

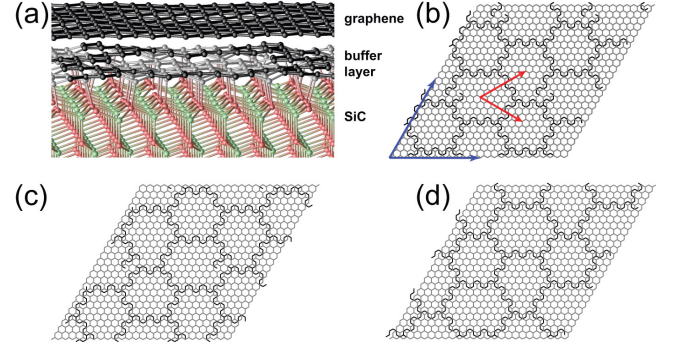


FIG. 1: (color online) (a) Ball and stick model for fully relaxed atomic configuration of epitaxial graphene, buffer layer and 4H-SiC (0001) surface with 6R3 supercell. Epitaxial graphene (black) is located on top of the buffer carbon atoms (black and grey). The buffer carbon atoms consisting 6  $\times$  6 domain are denoted by grey color and its boundary by black. The silicon and carbon atoms in the SiC are denoted by red and green respectively. (b)-(d) Coarse-grained minimal microscopic models. The red thick arrows indicate the 6  $\times$  6 supercell unit vectors and the blue ones 6R3 unit vectors. Black lines represent the connectivity of  $\pi$ -electrons of the buffer carbon atoms with approximate 6  $\times$  6 domain boundaries and grey lines denote the hexagonal network of epitaxial graphene on top of the buffer.

principles calculations (Fig. 2) (for detailed comparisons, see [34]). We notice that inclusion of the nearest neighbour interlayer interaction between graphene and the coarse-grained buffer layer model already breaks the symmetry between two sublattices of graphene. The simulated ARPES spectrum for monolayer epitaxial graphene agrees well with our previous results [22] from the first-principles calculation and ones [6, 7, 8, 9, 10] from experiments (Fig. 2) (for detailed ARPES simulation method, see [34]). When the initial conditions for the buffer layer formation are varied and the resulting geometries for the approximated 6  $\times$  6 domain are slightly altered as shown in Figs. 1(b)-(d), the simulated ARPES spectrum display essentially same structures with energy gaps at the  $E_D$ 's and the midgap states as shown in Figs 2(a)-(c). Hence, we confirm from the simple microscopic model that the sublattice symmetry-breaking interlayer interaction indeed opens a gap of 0.20 eV at the  $E_D$  and the presence of midgap states give rise to high ARPES intensities inside the energy gap as well as the level repulsion between upper and lower Dirac cones (Fig. 2(d)).

From simulated ARPES spectrum for bilayer epitaxial graphene, we find that the  $E_D$  approaches to the  $E_F$  and the energy gap decreases from 0.20 to 0.12 eV (Fig. 2(e)), agreeing well with experimental observations [7, 10, 17]. Due to the charge transfer between the SiC surfaces and graphene, perpendicular electric fields exist on the multilayer epitaxial graphene opening an energy gap [35, 36]. Though the fingerprints of midgap states are hardly visible for the bilayer epitaxial graphene, it is shown that

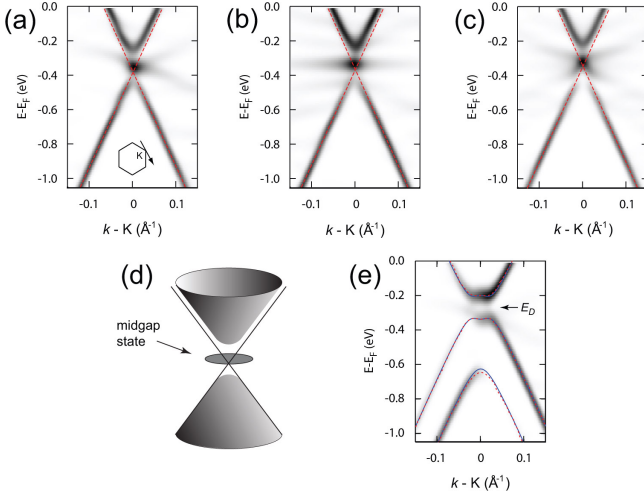


FIG. 2: (color online) Simulated ARPES spectrum near the  $E_D$  for various atomic models are drawn along the arrow shown in the inset of (a). The superimposed dotted lines are an ideal energy spectrum of graphene. Each simulated ARPES spectra in (a)–(c) corresponds to the geometry shown in Fig. 1 (b)–(d), respectively. The positions of  $E_D$  and size of energy gaps are (a) 0.35 eV, 0.20 eV, (b) 0.33 eV, 0.19 eV, and (c) 0.33 eV, 0.23 eV, respectively. (d) Schematic energy dispersion for epitaxial graphene with gap and midgap state. The straight lines are linear dispersion relations of ideal graphene. (e) Simulated ARPES spectra of bilayer epitaxial graphene near the  $E_D$ . Superimposed red and blue lines represent energy bands of bilayer graphene with and without buffer layer respectively. The position of  $E_D$  and energy gap are given by -0.26 eV and 0.12 eV respectively.

the interaction between the buffer and graphene attains the characteristic Mexican-hat-shaped band [35] at the bottom of the upper Dirac cone [Fig. 2(e) and Fig. 1S (c) in [34]] and shifts the second subband in the lower cone downward by 20 meV [Fig. 2(e)].

By simulating the two-dimensional ARPES intensity maps with various fixed energies (Fig. 3), we find that the interactions between the buffer layer and graphene indeed induce the symmetry breaking near the  $E_D$  and produce new hexagonal energy bands throughout the first BZ of graphene. Our simulated fixed-energy intensity patterns give a good agreement with experimental results [6, 7, 8, 9] (Fig. 3). Due to the two-source interference between photo-excited electrons from two equivalent atomic sites (a la Young's double slit) or helical nature of the carriers in graphene, the intensity patterns at the K-points show the typical crescent shape anisotropy [19]. With the characteristic high intensity at the K-points, there exist six equivalent faint replicas around each K-point forming a smaller hexagon (inset in Fig. 3(a)). When approaching  $E_D$ , the highest intensities at the K-points become isotropic and three of six replicas become weaker compared to other three points (inset in Fig. 3(b)). The intensities of stronger three satellites

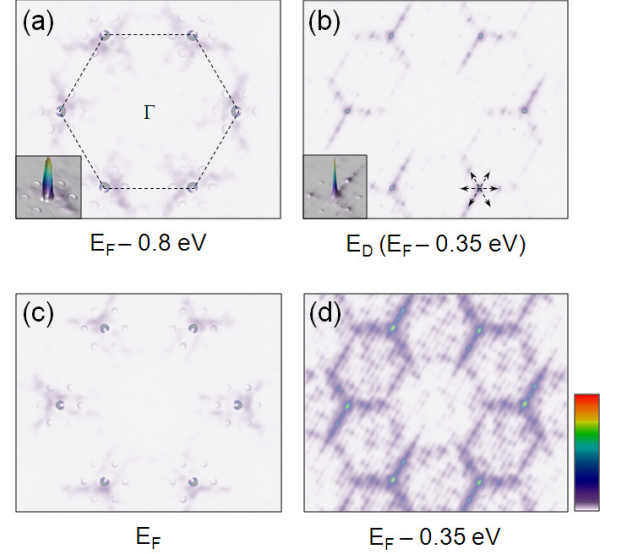


FIG. 3: (color online) Simulated ARPES intensity maps for constant energy taken on monolayer epitaxial graphene at (a) 0.8 eV (b) 0.35 eV ( $E_D$ ) and (c) 0.0 eV ( $E_F$ ) respectively. The first Brillouine zone of graphene is denoted by dotted line in (a). The insets in (a) and (b) show the stereographic plots near the  $E_D$ . The small arrows in (b) indicate the second shortest reciprocal lattice vectors of 6R3 supercell, which connect the K-point to six faint replicas. (d) Simulated ARPES intensity maps taken on buffer layer at 0.35 eV ( $E_D$ ) without graphene. The bar on the right side denotes the color scale of relative intensities from zero (white) to maximum (red).

amount to 7% of the main peak at the K-points while those of the weaker to 2% agreeing with experimental results qualitatively [7, 8, 9]. The replicas are connected by the second-shortest reciprocal lattice vectors of the 6R3 supercell (Fig. 3(b)) and the area of the smaller hexagon nearby is  $\frac{3}{13}$  of the first BZ of graphene [7]. When the interlayer interaction is set to zero intentionally in our simulation, we cannot find any symmetry breaking phenomena. Thus, we conclude that apparent six-fold symmetry breaking near the K-points is due to the interaction between the buffer and graphene. Together with six faint replicas, there are global faint features throughout the first BZ (Fig. 3(a)–(c)). We also find that the larger hexagonal structure around the  $\Gamma$ -point observed in the experiments [7, 8, 9] (25% of total area) originates from the buffer layer. By simulating constant energy map (Fig. 3(d)) and ARPES spectrum (Fig. 2S in [34]) of our coarse-grained buffer layer model, we show that the underlying faint features are reminiscent of the interlayer interactions between the buffer and graphene.

Usually, the surface of epitaxial graphene exhibits the finite-sized terrace patterns [8, 12, 28]. Thus the quantum confinement effect [32] may play a role in determining the energy gap [9]. To illustrate such an effect, we calculate electronic structures of epitaxial graphene

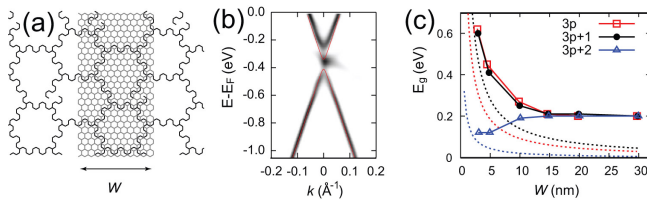


FIG. 4: (color online) (a) Atomic model for EAGNR of width  $W$  (here, 24-EAGNR is drawn) on top of the buffer layer. The lines follow the convention introduced in Fig. 1. (b) Simulated ARPES spectrum for nanoribbons with  $W = 19.9$  nm (163-EAGNR). The superimposed lines represent the energy band of 163-EAGNR having an energy gap of 0.72 eV without the buffer. (c) The energy gaps of  $N$ -EAGNRs as a function of width ( $N = 3p; 3p+1; 3p+2; p = \text{positive integer}$ ). The dotted lines correspond to energy energy gaps belong to each family without buffer layer.

nanoribbons with arm chair edges on both sides (in short, EAGNR) on top of the buffer layer. Following the convention [32], three families of EAGNRs are denoted by the number of dimer lines,  $N$ , i.e.,  $N$ -EAGNR ( $N = 3p, 3p+1, 3p+2$  families,  $p$  is a positive integer). By using the same model for the single layer epitaxial graphene (Fig. 4(a)), we show that the EAGNRs have a similar ARPES spectrum to epitaxial graphene for energy gaps, midgap states, and level repulsion between upper and lower cones, respectively (Fig. 4(b)). Moreover, when the width of EAGNR is over 15 nm, the typical family behaviour of energy gaps [32] disappears completely and converges to the energy gap (0.20 eV) of two-dimensional epitaxial graphene (Fig. 4(c)). Hence, we can conclude that the terrace patterns or finite-sized epitaxial graphene exhibit essentially the same electronic structures of the ideal two dimensional one. On the other hand, the present calculation results indicate that epitaxially grown graphene nanoribbons on the SiC surface will have the homogenous energy gap if the width is over 15 nm.

In summary, we have constructed the microscopic theory for epitaxial graphene on 4H-SiC (0001) surface incorporating interactions between graphene and the surface. The simulated experimental observations based on the theory have been shown to explain the several typical aspects of epitaxial graphene from a single and unified view and, thus, shed light on understanding the quasiparticle spectrum of graphene in various circumstances.

S.K. and J.I. acknowledge the support of the KOSEF through the SRC program (Center for Nanotubes and Nanostructured Composites). H.J.C. was supported by the KRF (KRF-2007-314-C00075) and by the KOSEF Grant No. R01-2007-000-20922-0. Y.-W.S. was supported by Quantum Materials Research Center No. R11-2008-053-01002-0 and Nano R&D program 2008-03670 through the KOSEF funded by the Korean government (MEST). Computational resources have been

provided by KISTI (KSC-2008-S02-0004) and the KIAS Linux Cluster System.

## SUPPLEMENTARY INFORMATION

### Construction of minimum model Hamiltonian within tight-binding approximations

In first-principles calculations, we expand the wave function with localized basis sets [22, 33] to handle a large number of atoms in the system (typically  $> 1600$  atoms). A single- $s$  for hydrogen, a single- $s$  plus polarization for silicon and a mixed basis set with a single and double- $s$  for  $s$ - and  $p$ -orbitals of carbon atom have been used, respectively [22]. The Kleinman-Bylander's fully separable nonlocal projectors [37] are used in the norm-conserving pseudopotentials [38] and the local density approximation [39] is employed in setting up the exchange-correlation potential. We have thoroughly tested our basis set with other calculation parameters to reproduce the atomic and electronic structures of SiC, graphene, other model for epitaxial graphene studied in previous literatures [20, 21, 23], respectively. We modeled the 4H-SiC (0001) substrate in the simulation with four alternating silicon and carbon atomic layers. Hydrogen atoms are introduced to passivate the dangling bonds in bottom of the slab. On top of the Si-terminated surface of 4H-SiC (0001), one, two, and three graphene layers are placed for the buffer layer, monolayer graphene, and bilayer graphene, respectively.

Based on the low energy electron diffraction (LEED) experiments [4, 29, 31], the large supercell with the  $6\sqrt{3} \times 6\sqrt{3} \times 30$  (in short 6R3) periodicity (equivalent to  $13 \times 13$  times graphene unit cell) is imposed to the calculations. The atomic positions are determined by total energy minimization calculations until the forces on each atom are less than 0.06 eV/Å while atoms belonging to the last two silicon and carbon layers are fixed to the bulk atomic structure of 4H-SiC. In the electronic structure calculations after geometric optimization process, we use  $2 \times 2$   $k$ -point sampling in lateral directions and set very large size of vacuum (50 Å) in surface normal direction to prevent the spurious dipolar interactions between terminated slab geometries in supercell construction.

During the high temperature thermal decomposition process [4, 6, 7, 17, 18, 29, 31], the detailed atomic structures and shape of the domain may vary from sample to sample. However, the domain boundary of  $s$ -orbitals of the buffer carbon atoms and the exact 6R3 periodicity remains the same as observed in many experiments [4, 6, 7, 17, 18, 29, 31] and shown in our calculations [22]. Hence, it is sufficient to approximate the buffer layer to the coarse-grained atomic configuration of the quasi- $6\sqrt{3} \times 6\sqrt{3}$  periodic connections of  $s$ -electrons only. We also found from the first-principles calculations that



the interactions between  $\pi$ -orbital states at the domain boundary of the buffer and ones in graphene play the most significant role to determine the electronic structures of the system [22]. It is also noticeable that electronic states of atoms inside the domain and those under the buffer layer have negligible contributions.

Hence, based on results from the first-principles calculations, our tight-binding Hamiltonian for monolayer epitaxial graphene on coarse-grained buffer layer model (Fig. 1 (b)-(d)) can be written as

$$H = \sum_{\langle i,j \rangle} t_G c_i^\dagger c_j + \sum_{\langle i,j \rangle} V_G c_i^\dagger c_j + \sum_{\langle i,j \rangle} t_B b_i^\dagger b_j + \sum_{\langle i,j \rangle} V_B b_i^\dagger b_j + (c.c.); \quad (2)$$

where  $t_G$  ( $= 2.70\text{eV}$ ) and  $t_B$  ( $= 1.50\text{eV}$ ) are the nearest neighbour hopping amplitude between carbon atoms in graphene and those in the buffer layer respectively. The  $c_i$  and  $b_i$  are annihilation operators for electron in graphene and buffer layer respectively. ( $= 0.30\text{eV}$ ) denotes the interlayer hopping amplitude between the nearest neighbour carbon atoms belong to graphene and the buffer layer with the Bernal type stacking respectively.  $V_G$  ( $= 0.35\text{eV}$ ) and  $V_B$  ( $= 0.34\text{eV}$ ) describe the potential for graphene and the buffer layer considering charge redistributions due to the polar SiC surface. These parameters were found to be enough for fitting our first-principles energy bands of the buffer layer and monolayer epitaxial graphene, respectively (Fig. 1S (a) and (b))

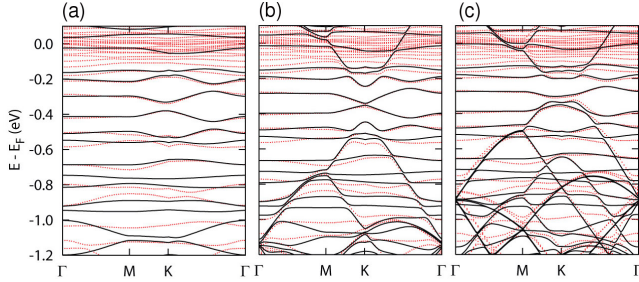


FIG. 5: Comparison between electronic energy bands from the first-principles calculation and tight-binding approximation. Electronic energy bands of (a) the buffer layer on top of 4H-SiC (0001) slab model, (b) monolayer epitaxial graphene and (c) bilayer epitaxial graphene on top of the buffer layer with 4H-SiC (0001) slab, respectively. The spectrum are drawn along the high symmetric lines of the first Brillouin zone of 6R3 supercell. The dotted red lines are obtained by the first-principles calculations on the atomic models including one (two) graphene layer, buffer layer, and 4H-SiC (0001) slab. The solid black lines are obtained by our microscopic model Hamiltonian within the tight-binding approximations (Eq. 1). It is found that the dense flat bands near the Fermi levels are from the states isolated inside the approximate 6  $\times$  6 domains of the buffer layer and SiC surface underneath it, which do not contribute to ARPES intensities.

while the second and third nearest neighbour interlayer interaction terms improve the agreements a little.

For bilayer epitaxial graphene, we introduce another interlayer hopping amplitude between the nearest neighbours carbon atoms belong to each graphene layer (Bernal type stacking) and potential shifts for each graphene layer,  $V_G$  and  $V_G^0$  with respect to the Fermi level. The Hamiltonian for the interaction is written as  $H^0 = H_0 + H_1$ , where

$$H_1 = \sum_{\langle i,j \rangle} t_G d_i^\dagger d_j + \sum_i V_G^0 d_i^\dagger d_i + \sum_{\langle i,j \rangle} c_i^\dagger d_j + (c.c.); \quad (3)$$

Here,  $d_i$  is the annihilation operator for electron in second graphene. We fit the energy spectrum of bilayer epitaxial graphene obtained by our model Hamiltonian to the first-principles calculation results (Fig. 1S (c)) and found  $t = 0.35\text{eV}$  being quite similar to one of graphite, but smaller than 0.48 eV [17] and 0.46 eV [18] obtained in recent experiments.

As shown in Fig. 1S, the agreements between energy spectrum obtained by the first-principles calculations and ones by our model Hamiltonians are excellent. The dense flat bands near the Fermi level in Fig. 1S from the first-principles calculations are found to originate from localized states inside approximate 6  $\times$  6 domains of the buffer layer and localized states in 4H-SiC (0001) surfaces underneath the buffer. We found that such localized states forming flat bands are buried deep inside the surfaces and do not contribute to the simulated ARPES spectrum.

#### Simulation of angle resolved photoemission spectroscopy (ARPES) intensities

We use the Fermi golden rule to simulate ARPES spectra [19, 40]. The transition probability ( $I$ ) from an initial Bloch state ( $i$ ) to an outgoing electron state ( $f = e^{ip}$ ) is written as

$$I = \hbar^{-1} | \langle f | H_{ph-el} | i \rangle |^2 (\hbar\omega + E_i - E_f) \quad (4)$$

where  $H_{ph-el}$  is the photon-electron interaction Hamiltonian,  $\hbar\omega$  is the frequency of incident photon, and  $E_{i(f)}$  is an energy of  $i(f)$ . Tight-binding wavefunction obtained for the system is given by,

$$|i\rangle = \sum_j a_j(k) \frac{1}{N} \sum_T \psi_j(r - x_j - T) e^{ik \cdot T} \quad (5)$$

where  $a_j(k)$  is an amplitude for the  $\pi$ -orbital located at  $x_j$  in the 6  $\times$  3  $\times$  6  $\times$  3R30 supercell with unit vector  $T$  and  $k$  is the crystal momentum of electron.

By using the dipole approximation,  $H_{ph-el} \propto A e^{iq \cdot x}$ , the transition probability will be expressed as

$$I(p) = \sum_i \sum_j a_i(k) e^{ip \cdot x_i} (\hbar\omega + E_i - E_f) \quad (6)$$

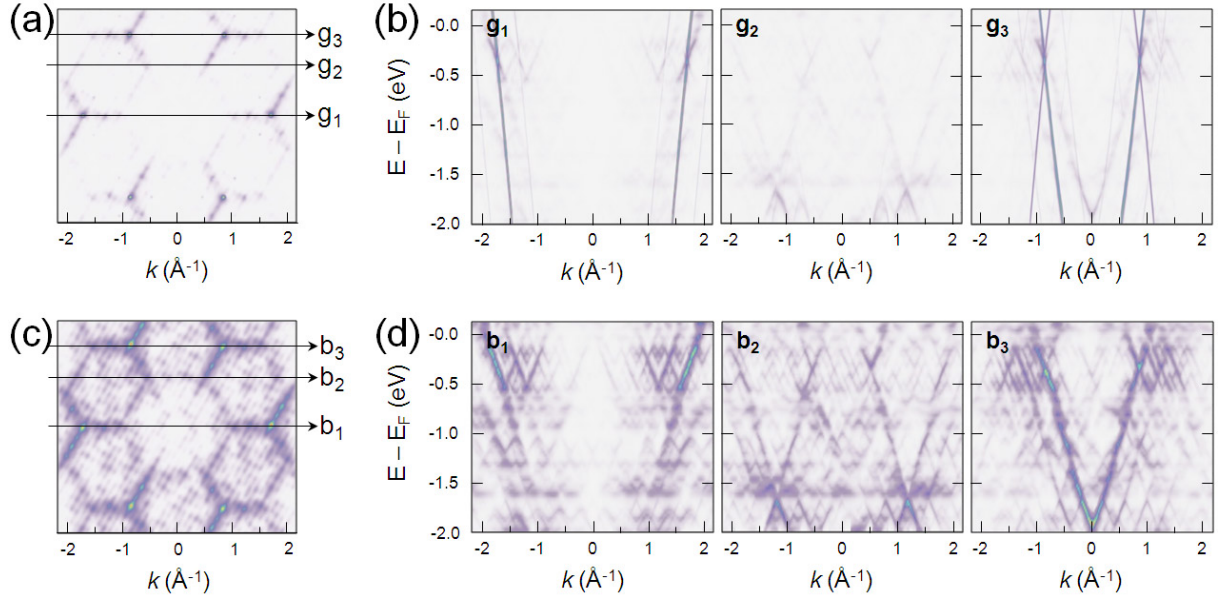


FIG. 6: Simulated energy spectrum of epitaxial graphene and buffer layer along various directions in the first Brillouine zone of graphene. (a) Simulated ARPES intensity map taken on monolayer epitaxial graphene at the Dirac energy point ( $E_D$ ). (b) From left to right panels, simulated ARPES spectrum along the  $g_1$ ,  $g_2$  and  $g_3$  shown in (a) respectively. Together with strong ARPES intensities from graphene, there are several dispersions originating from the buffer layer. (c) Simulated ARPES intensity map taken on minimal buffer layer model at the  $E_D$ . (d) From left to right panels, simulated ARPES spectrum along the  $b_1$ ,  $b_2$  and  $b_3$  shown in (c) respectively. It is noticeable that all characteristic ARPES spectrum of the buffer shown in each panel of (d) appears faintly in the corresponding one of (b), respectively.

where  $\mathbf{p}$  is the momentum of outgoing electron and  $\mathbf{p}_j$  is the Fourier transformation of atomic orbital  $\phi_j(\mathbf{r})$ , defined by  $\mathbf{p}_j = \int \mathbf{r} \phi_j(\mathbf{r}) e^{-i\mathbf{p}_j \cdot \mathbf{r}} d\mathbf{r}$  (set by constant). The crystal momentum  $\mathbf{p}$  belong to the first Brillouin zone of the  $6\sqrt{3} \times 6\sqrt{3} R_{30}$  supercell and satisfies momentum conservation condition in the surface parallel direction (i.e.,  $\mathbf{k} + \mathbf{G} = \mathbf{p}_{jj}$  for the reciprocal vector  $\mathbf{G}$ ) of the supercell. We include the attenuation factor for the ARPES intensity considering photoelectron mean free path ( $\sim 5\text{\AA}$ ) to the surface normal direction. The conservation of energy imposed by the  $\delta$ -function is replaced by Lorentzian function,  $\frac{1}{(\hbar\omega + E_i - E_f)^2 + \gamma^2}$ , with a broadening ( $\gamma$ ) of 30 meV. We simulate the ARPES spectrum (shown in Figs. 2 and 4(b)) with a photon energy of 50 eV and the two-dimensional constant energy maps (shown in Fig. 3 and Fig. 2S) with a photon energy of 100 eV [6, 7].

Present Address: The Makineni Theoretical Laboratories, Department of Chemistry, University of Pennsylvania, Philadelphia, PA 19104, USA

<sup>y</sup> Electronic address: hand@kias.re.kr

- [1] K. S. Novoselov et al, Science 306, 666 (2004).
- [2] K. S. Novoselov et al, Nature 438, 197 (2005).
- [3] Y. Zhang, Y.-W. Tan, H. L. Stormer, and P. Kim, Nature 438, 201 (2005).
- [4] C. Berger et al, Science 312, 1191 (2006).

- [5] A. K. Geim and K. S. Novoselov, Nature Mat. 6, 183 (2007).
- [6] A. Bostwick et al, Nature Phys. 3, 36 (2007).
- [7] S. Y. Zhou et al, Nature Mat. 6, 770 (2007).
- [8] E. Rotenberg et al, Nature Mat. 7, 258 (2008).
- [9] S. Y. Zhou et al, Nature Mat. 7, 259 (2008).
- [10] D. S. Lee et al, Nano Lett. 8, 4320 (2008).
- [11] P. Mallet et al, Phys. Rev. B 76, 041403(R) (2007).
- [12] T. Ohta et al, New J. Phys. 10, 023034 (2007).
- [13] A. Bostwick et al, New J. Phys. 9, 385 (2007).
- [14] L. Vitali et al, Surf. Sci. 602, L120 (2008).
- [15] I. Brihuega et al, Phys. Rev. Lett. 101, 206802 (2008).
- [16] J. Hass, J. E. Millan-Otoya, P. N. First, and E. H. Conrad, Phys. Rev. B 78, 205424 (2008).
- [17] T. Ohta et al, Phys. Rev. Lett. 98, 206802 (2007).
- [18] P. Laufer et al, Phys. Rev. B 77, 155426 (2008).
- [19] M. M. Uchak-Kuczyński et al, Phys. Rev. B 77, 195403 (2008).
- [20] A. M. Attouch and O. Pankratov, Phys. Rev. Lett. 99, 076802 (2007).
- [21] F. Varchon et al, Phys. Rev. Lett. 99, 12805 (2007).
- [22] S. Kim, J. Ihm, H. J. Choi, and Y.-W. Son, Phys. Rev. Lett. 100, 176802 (2008).
- [23] F. Varchon, P. Mallet, J.-W. Veuille, and L. Magaud, Phys. Rev. B 77, 235412 (2008).
- [24] L. Benfatto and E. Cappelluti, Phys. Rev. B 78, 115434 (2008).
- [25] P. E. Trevisanutto et al, Phys. Rev. Lett. 101, 226405 (2008).
- [26] C.-H. Park et al, Phys. Rev. Lett. 102, 076803 (2009).
- [27] R. M. Tromp and J. B. Hannon, Phys. Rev. Lett. 102,

- 106104 (2009).
- [28] K. V. Emtsev et al., et al., *Nature Mat.* 8, 203 (2009).
  - [29] W. A. de Heer et al., *Solid State Commun.* 143, 92 (2007).
  - [30] K. V. Emtsev et al., *Mater. Sci. Forum* 556-557, 525 (2007).
  - [31] W. Chen et al., *Surf. Sci.* 596, 176 (2005).
  - [32] Y.-W. Son, M. L. Cohen, and S. G. Louie, *Phys. Rev. Lett.* 97, 216803 (2006).
  - [33] J. M. Soler et al., *J. Phys. Condens. Matter* 14, 2745 (2002).
  - [34] For detailed calculation methods, see Supplementary Information.
  - [35] E. McCann, *Phys. Rev. B* 74, 161403(R) (2006).
  - [36] T. Ohta et al., *Science* 313, 951 (2006).
  - [37] L. Kleinman and D. M. Bylander, *Phys. Rev. Lett.* 48, 1425 (1982).
  - [38] N. Troullier and J. L. Martins, *Phys. Rev. B* 43, 1993 (1991).
  - [39] D. M. Ceperley and B. J. Alder, *Phys. Rev. Lett.* 45, 566 (1980).
  - [40] A. R. Damascelli, Z. Hussain, Z.-X. Shen, *Rev. Mod. Phys.* 75, 473 (2003).